Enhancing the Supercapacitive Properties of Iron Oxide Electrode through Cu^{2+}-doping: Cathodic Electrosynthesis and Characterization

Mustafa Aghazadeh[1], Mohammad Ghannadi Maragheh[1] and Parviz Norouzi[2,3,*]

[1] Materials and Nuclear Research School, Nuclear Science and Technology Research Institute (NSTRI), P.O. Box 14395-834, Tehran, Iran
[2] Center of Excellence in Electrochemistry, School of Chemistry, College of Science, University of Tehran, Tehran, Iran
[3] Biosensor Research Center, Endocrinology and Metabolism Molecular-Cellular Sciences Institute, Tehran University of Medical Sciences, Tehran, Iran
[*]E-mail: norouzi@khayam.ut.ac.ir

Cu^{2+} doped iron oxide nanoparticles (Cu-IONPs) are prepared *via* a one-step facile electrodeposition procedure. In this procedure, Cu-IONPs are electro-deposited in a two-electrode set up from an additive-free aqueous solution of mixed $Fe(NO_3)_3$, $FeCl_2$ and $CuCl_2$ salts. The applied deposition parameters were current density of 10 mA cm^{-2}, bath temperature of 25°C and deposition time of 30 min. The structural and morphological characterizations through X-ray diffraction (XRD), field emission electron microscopy (FE-SEM) and energy-dispersive X-ray (EDX) confirmed that the fabricated Cu-IONPs sample is composed of Cu^{2+} doped magnetite phase with particles with average size of 20 nm. Magnetic studies by VSM showed that the deposited Cu-IONPs provide proper super-paramagnetic characters of saturation magnetization(Ms=54.47 emu g^{-1}), remanent magnetization *(Mr)* *(Mr*=0.41 emu g^{-1}) and coercivity (H_{Ci}=10.53 G). The obtained electrochemical data indicated that Cu-IONPs are enable to exhibit specific capacitance as high as 189.6 F g^{-1} at a discharging current of 2 A g^{-1}, and 88.8% capacity retention after 2000 GCD cycling. Based on the obtained results, our developed electrosynthesis method is proposed as a facile route for the synthesis of high performance Cu-IONPs.

1. INTRODUCTION

One of the power storage devices which plays an important roles in energy storage is electrochemical capacitors (ECs). Compare to other energy storage, they possess high charge/discharge

rate, tremendous reversibility and long cycle life [1]. ECs are classified to electric double layer capacitors (EDLCs) and pseudocapacitors (PCs) according to their charge/discharge manner. EDLCs store the charge through non-faradaic process in which an electrical double layer forms due to the charge separation between electrode surface and ionic solution. While PCs store the charge through a faradaic process in which redox reactions occur due to the electroactive materials in the electrode [2]. Generally, the pseudocapacitors can provide higher specific power and longer cycle life compared to EDLCs. Electro-active materials in SC electrode are its main determining part. Therefore, many researches have been performed to discover high performance electrode materials. For PCs, nanomaterials like as cobalt oxide [3-5], copper oxide [6], nickel oxide [7,8], manganese oxides [9-13], cobalt hydroxide [14-17], nickel hydroxide [18-22], hematite [23-25] and magnetite [26-28] have been reported as most proper candidates. Among these interested materials, magnetite (Fe_3O_4) has attracted much attention due to their changeable oxidation states, natural abundance, inexpensiveness, and eco-friendly [29]. However, charge storage ability of pure magnetite electrode is significantly restricted by reason of its intrinsically low electrical conductivity, which exclude its widespread application in commercial SCs [30,31]. Until now, the strategies of (i) mixing composite with carbon-based material [32-35], (ii) doping with metal ions [36], and (iii) planning novel nanostructures [37-44] have been applied to improve the capacitive ability of iron oxide electrode. Among these solution ways, metal ion doping strategy has been rarely investigated. Here, we introduce a facile route for the synthesis of metal ion (Cu^{2+}) doped iron oxide nanoparticles (Cu-IONPs) through cathodic electro-deposition (CED) procedure, and also observed that 20% improvement in supercapacitive performance of Cu-IONPs could be achieved through Cu^{2+} doping. This procedure use the cathodic electrosynthesis route. In this method, nanostructured metal oxides/hydroxides such as $Co(OH)_2$, $Ni(OH)_2$, Mn_3O_4 and NiO could be fabricated through base generation on the cathode surface [45-47]. However, this procedure has not been used in the preparation iron oxide nanoparticles (IONPs). It is worth noting that we very recently reported one-pot CED fabrication of IONPs [48-51]. Here, we applied a CED strategy for the synthesis of Cu^{2+} doped Fe_3O_4 NPs. It is worth noting that cathodic deposition of Cu^{2+} doped Fe_3O_4 NPs has not been studied until now. The prepared Cu-IONPs were investigated by XRD, FE-SEM, VSM, cyclic voltammetry (CV) and galvanostatic charge-discharge (GCD) techniques. The obtained data proved the suitable magnetic and supercapacitive behavior of the prepared Cu^{2+} doped Fe_3O_4 nanoparticles.

2. EXPERIMENTAL PROCEDURE

2.1. Materials

$FeCl_2 \cdot 4H_2O$, $Fe(NO_3)_3.9H_2O$, $CuCl_2.2H_2O$ and polyvinylidene fluoride (PVDF, $(CH_2CF_2)_n$) were purchased from Sigma Aldrich. All materials were used as received, without any purification.

2.2. Electrosynthesis of Cu^{2+} doped Fe_3O_4 NPs

The cathodic electrosynthesis (CE) procedure previously used for the electrosynthesis of naked and coated magnetite nanoparticles (MNPs) [51-56], was here applied for the preparation of Cu^{2+}

doped Fe_3O_4 NPs. Fig. 1 presents a deposition procedure . The preparation system was included of a (316 L, 5cm×5cm×0.5mm) steel cathode centered between two parallel graphite anodes, as shown in Fig. 1. The electrolyte solution was prepared by mixing (2g) $Fe(NO_3)_3 \cdot 9H_2O$, (1g) $FeCl_2 \cdot 4H_2O$ and (0.3g) $CuCl_2 \cdot 2H_2O$ in 1 liter aqueous solution. The electrodeposition runs were conducted on an electrochemical workstation system (Potentiostat/Galvanostat, Model: NCF-PGS 2012, Iran) with applying 10mA cm^{-2}. The deposition time and bath temperature were 30 min and 25 ^{o}C, respectively.
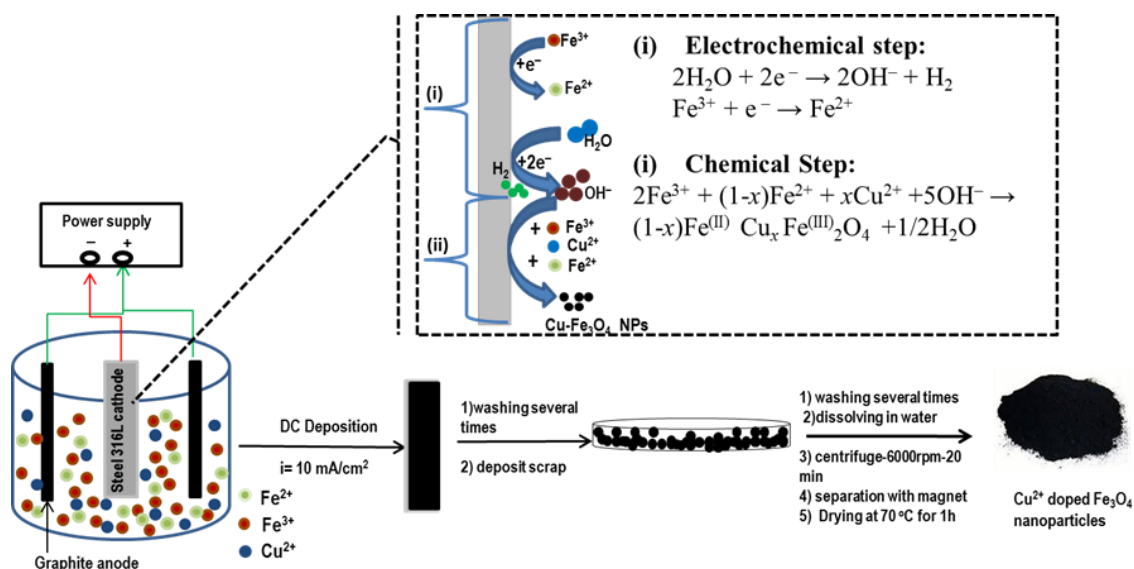
Figure 1. Schematic view of the electrosynthesis of Cu^{2+} doped Fe_3O_4 nanoparticles. The inset presents (i) electrochemical and (ii) chemical steps of Cu^{2+} doped Fe_3O_4 formation on the cathode surface.

After each deposition run, the cathode was bring out from solution and rinsed several times with deionized H_2O. Then, the deposited black film was scraped form the steel and subjected to separation and purification steps, as noted in Fig. 1;(i) the obtained wet powder was dispersed in deionized water and centrifuged at 6000rpm for 20min to removal of free anions, as indicated in Fig. 1,(ii) the deposit was then separated from water solution by a magnet, dried at 70 ^{o}C for 1h, and (iii) the resulting black dry powder was named Cu-IONPs, and used for further evaluations.

2.3. Characterization analyses

The SEM images of the prepared powder were provided through field-emission scanning electron microscopy (FE-SEM, Mira 3-XMU with accelerating voltage of 100 kV). The crystal structure of the prepared powder was determined by X-ray diffraction (XRD, Phillips PW-1800) using a Co Kα radiation. The magnetic properties of the prepared Cu^{2+} doped Fe_3O_4 nanoparticles were assessed in the range of −20000 to 20000 Oe at room temperature using vibrational sample magnetometer (VSM, Meghnatis Daghigh Kavir Co., Iran).

2.4. Electrochemical tests

Cyclic voltammetry (CV), galvanostatic charging/discharging (GCD) and electrochemical impedance spectroscopy (EIS) were used for electrochemical characterization of the prepared samples. These tests were done using an electrochemical station (AUTOLAB®, Eco Chemie, PGSTAT 30)in a three-electrode set up containing a Na_2SO_3 (1 M) aqueous electrolyte. The three-electrode set-up was composed of working electrode (Cu^{2+} doped Fe_3O_4 nanoparticles paste electrode), Ag/AgCl reference electrode (saturated with 1 M KCl), and a counter electrode (platinum wire). The working electrode (WE) was fabricated through the well-known paste procedure [23,26]; First, the prepared black Cu-IONPs powder was physically mixed with acetylene black (>99.9%) and conducting graphite (with rations of 75:10:10), and the mixture was homogenized properly. Then, 5 wt% polyvinylidene fluoride (PVDF) dissolved inN-Methyl-2-pyrrolidone (NMP) was added into the mixture. After partially evaporating the NMP content of the mixture, the resulting paste was pressed at 10 MPa onto Ni foam (surface area of $1cm^2$). The resulting electrode was dried for 5 min at about 150 °C in oven. In final, the fabricated electrode was used as working electrode in the electrochemical tests. The mass loading of Cu-IONPs powder onto the Ni foam was about 2.4 mg. The CVs of the fabricated working electrode were recorded in a 1M Na_2SO_3 electrolyte in the potential range of -1.0 to+0.1 V vs. Ag/AgCl. The CV profiles were recorded at the potential sweeps of 2, 5, 10, 20, 50 and 100 mV s^{-1}. The GCD curves were recorded at the different current loads of 0.5, 1, 2, 3 and 5 A g^{-1} within a potential range of -1.0 to 0V vs. Ag/AgCl. The specific capacitances were calculated from the CVs and GCD curves according to the equations [13,14]:

$$C = \frac{Q}{m\Delta V}, Q = \int_{V_a}^{V_a} I(V)\,dV \qquad (1)$$

$$C = \frac{Q}{m \times \Delta V}, Q = I \times \Delta t \qquad (2)$$

where C is the capacitance of prepared Cu-IONPs powder (F g^{-1}), Q is the total charge, ΔV is the potential window, *m* is the mass of Cu-IONPs powder (g), v is the scan rate (V s^{-1}), I(V) is the current response during the potential scan, I is the applied current load (A) and Δt is the time of a discharge cycle. Furthermore, the energy and power densities (E and P) were calculated by the equation [28]:

$$E = [C(\Delta V)^2]/2 \qquad (3)$$

$$P = E/\Delta t \qquad (4)$$

where E, C, ΔV, P and Δt are the specific energy, specific capacitance, potential window, specific power and discharge time, respectively.

3. RESULTS AND DISCUSSION

3.1. Structural and morphological characterizations

Fig. 2 shows the XRD patterns of electro-synthesized undoped and Cu^{2+} doped Fe_3O_4powder. All the observed diffraction peaks in the XRD patterns could be readily referred to the pure cubic phase [space group: Fd3m (227)] of Fe_3O_4 with cell constants $a = 8.389$ Å (JCPDS 01-074-1910).
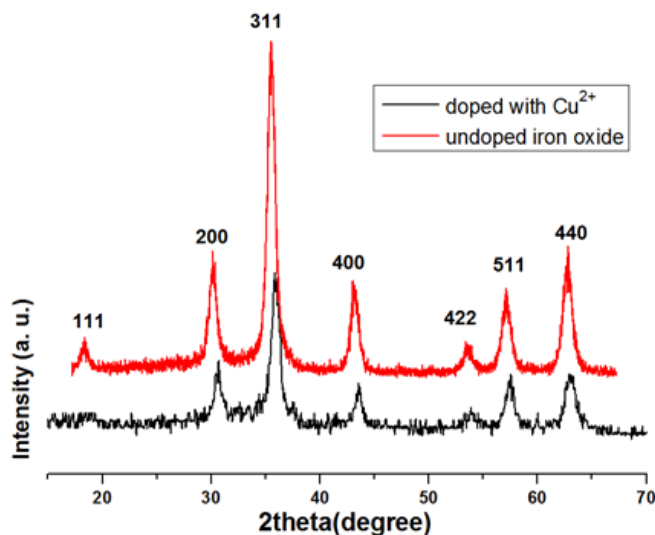
Figure 2. XRD patterns of undoped and Cu^{2+} doped Fe_3O_4 nanoparticles.

There is no extra peak in XRD pattern indicating purity magnetite phase of the electro-synthesized Cu-IONPs. This result implicates that the magnetite structure is formed on the steel surface at our applied CE conditions, and hence it can be said that Cu^{2+} cations play a same role of Fe^{2+} cations during CE process. It was established that CE deposition of metal hydroxides/oxide is taken placed through two-step process i.e. electrochemical and chemical steps [45,51,52]:

Electrochemical step:

$$2H_2O + 2e^- \rightarrow 2OH^- + H_2 \qquad (5)$$

Chemical step:

$$(1-x)Fe^{2+} + xCu^{2+} + 2Fe^{3+} + 5OH^- \rightarrow Fe^{(II)}_{(1-x)}Cu_xFe^{(III)}O_4 + 1/2H_2O \qquad (6)$$

The Cu^{2+} cations are incorporated into the Fe_3O_4 crystal structure through occupation of some sites related to the Fe^{2+} cations. And the Cu^{2+} doped Fe_3O_4 is resulted as the CE product on the cathode surface.
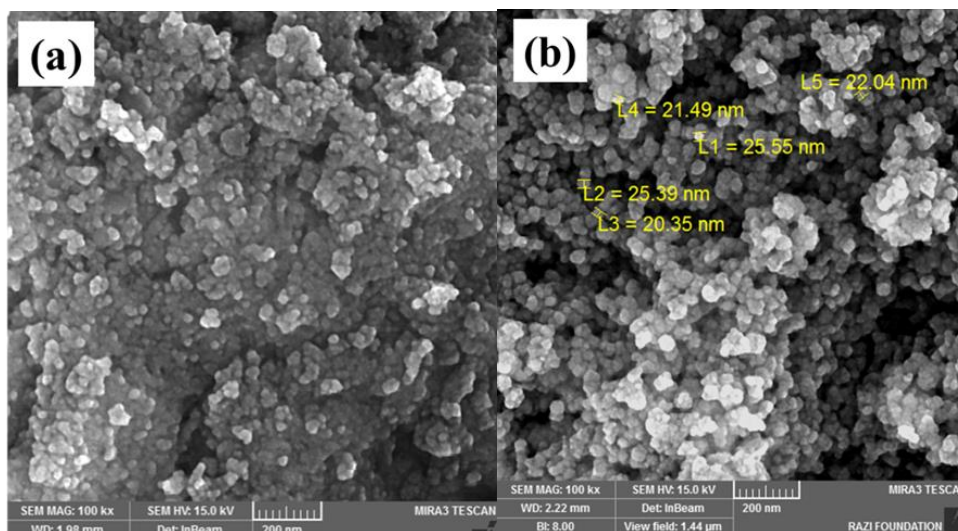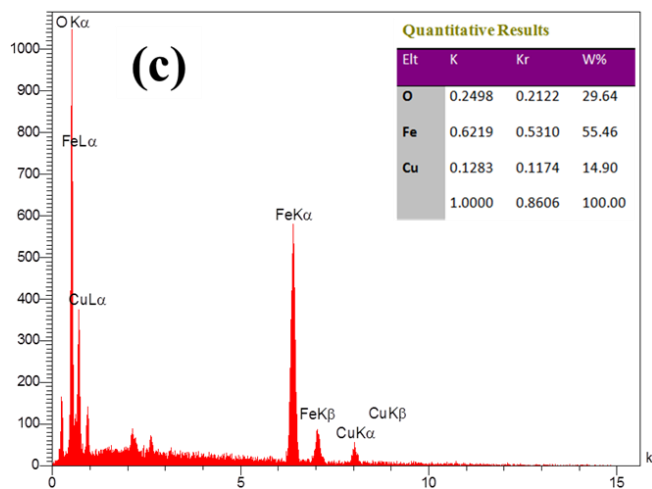
Figure 3. FE-SEM images of (a) undoped and (b) Cu^{2+} doped Fe$_3$O$_4$ nanoparticles and (c) EDS data for doped sample.

The average crystallite size (D) of the Cu-IONPs was calculated using the Debye–Scherrer equation, D=0.9λ/βcos(θ), where λ is the X-ray wavelength, β is the full width at half maximum of the diffraction line, and θ is the diffraction angle of the XRD pattern. From the diffraction line-width of (311) peak, the average crystallite size of the prepared Cu-IONPs was calculated to be 11.6 nm.

Figs. 3a and b presents FE-SEM images of the electrosynthesized undoped and Cu^{2+} doped IONPs. It is clearly seen that the prepared IONPs have spherical texture with the particles size of 20-25nm (Figs. 3a and b). The elemental analysis of the prepared IONPs was studied by energy-dispersive X-ray (EDX), which is presented in Fig. 3c. In this data, it is seen that the synthesized Cu-IONPs have the Fe (55.46%wt), Cu (14.9%wt) and O (29.64%wt) elements. With considering the fact that Cu^{2+} cations plays a same role of Fe^{2+} cations in the CE process, these values are matched with the weight percentages of Fe(72.36%wt) and O (27.64%wt) in the Fe$_3$O$_4$chemical formula. These values implicated the deposition of Fe$_3$O$_4$NPs doped with ~15% Cu^{2+} through our developed CE strategy.
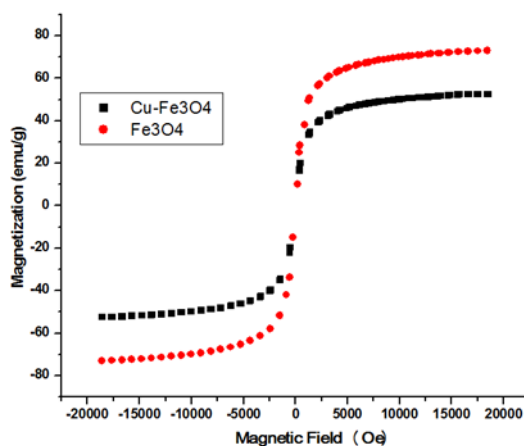
Figure 4. Hysteresis loops for undoped and Cu^{2+} doped iron oxide nanoparticles.

The magnetic hysteresis loops for the prepared Cu-IONPs and IONPs are shown in Fig. 4. No hysteresis is seen in the VSM profiles and the curves have S like form, as seen in Fig. 4. These observations implicated that the prepared Cu-IONPs have superparamagnetic behavior. The magnetic data of the prepared Cu-IONPs are listed in Table 1.

Table 1. Magnetic data of the undoped and Cu^{2+} doped iron oxide nanoparticles

Sample name	Ms(emu/)g	Coercivity (Hci) G	Positive (Hci) G	Negative (Hci) G	Negative Mr(emu/g)	Positive Mr(emu/g)	Retentivity Mr(emu/g)
IONPs	72.96	14.6	-41.87	-12.66	0.83	2.73	0.95
Cu-IONPs	52.49	3.09	-5.92	-12.09	-0.24	0.51	0.02

For the electrosynthesized Cu-IONPs, the magnetic data i.e. saturation magnetization (*Ms*), remanent magnetization (*Mr*) and coercivity (H_{Ci}) are observed to be; *Ms*=52.49 emu g^{-1}, *Mr*=0.02 emu g^{-1} and H_{Ci}=13.09 G. These data confirmed the superparamagnetic nature of the electrosynthesized Cu-IONPs. Also, our Cu-IONPs exhibit better superparamagnetic characteristics i.e. higher *Ms* and lower *Mr* and *Hci* values as compared with those reported in the literature i.e. Sm^{3+} doped IONPs(*Ms*=31.3 emu g^{-1} and *Hci*=85.7 G) [57], Eu^{3+} doped IONPs(*Ms*=23.6 emu g^{-1} and *Hci*=74.3 G) [58], Gd^{3+} doped IONPs(*Ms*=of 32.9 and 28.9 emu g^{-1} at 100 and 300 K) [59], and Cu^{2+} doped IONPs (*Ms*=53.2 emu g^{-1} and *Hci*=25.3 G) [60], and Mn^{2+} doped IONPs (*Ms*=61.5 emu g^{-1} and *Hci*=34.5 G) [60]. Furthermore, these magnetic data are comparable with those of undoped IONPs electro-synthesized at a similar electrochemical condition in our previous works. The hysteresis behavior of undoped IONPs have been previously studied by the authors, and the reported data are *Ms* = 72.96 emu g^{-1}, *Mr*=0.95emu g^{-1}, positive *Mr* =2.73 emu g^{-1}, negative *Mr*=-0.83 emu g^{-1} and H_{Ci}=14.61 G [54,55]. The Cu^{2+} doped Fe_3O_4 nanoparticles exhibited low *Ms* compared with undoped Fe_3O_4 nanoparticles, which can be connected to the Cu atoms low magnetism compared with Fe ones. However, Cu^{2+} doped Fe_3O_4NPs show smaller *Mr* and H_{Ci} values as compared with the undoped IONPs, which implicated their better superparamagnetic nature. Therefore, it can be said that Cu^{2+} doping improves magnetic character of IONPs.

3.2. Electrochemical evaluation

3.2.1. Cyclic voltammetry

Cyclic voltammetry was used to evaluate the charge storage ability of the working electrode (WE) fabricated from the prepared Cu^{2+} doped Fe_3O_4 nanoparticles and comparison with undoped Fe_3O_4. Fig. 5a presents the CV profiles of the prepared WE within the voltage window of -1.0 to +0.1V vs. Ag/AgCl with applying the scan rates of 2-100 mV s^{-1}. The shapes of the CV curves clearly reveal the pseudocapacitive characteristics of the Cu-IONPs, which is different from the electric double-layer capacitance. In the literature, a combination of both EDLC and pseudocapacitance

including the reduction/oxidation of specifically adsorbed SO_3^{2-} anions on the Fe_3O_4 surface has been observed for the capacitance behavior of pure Fe_3O_4 electrode in the Na_2SO_3 solution [29-34], which are seen by small peaks on the CV curve.
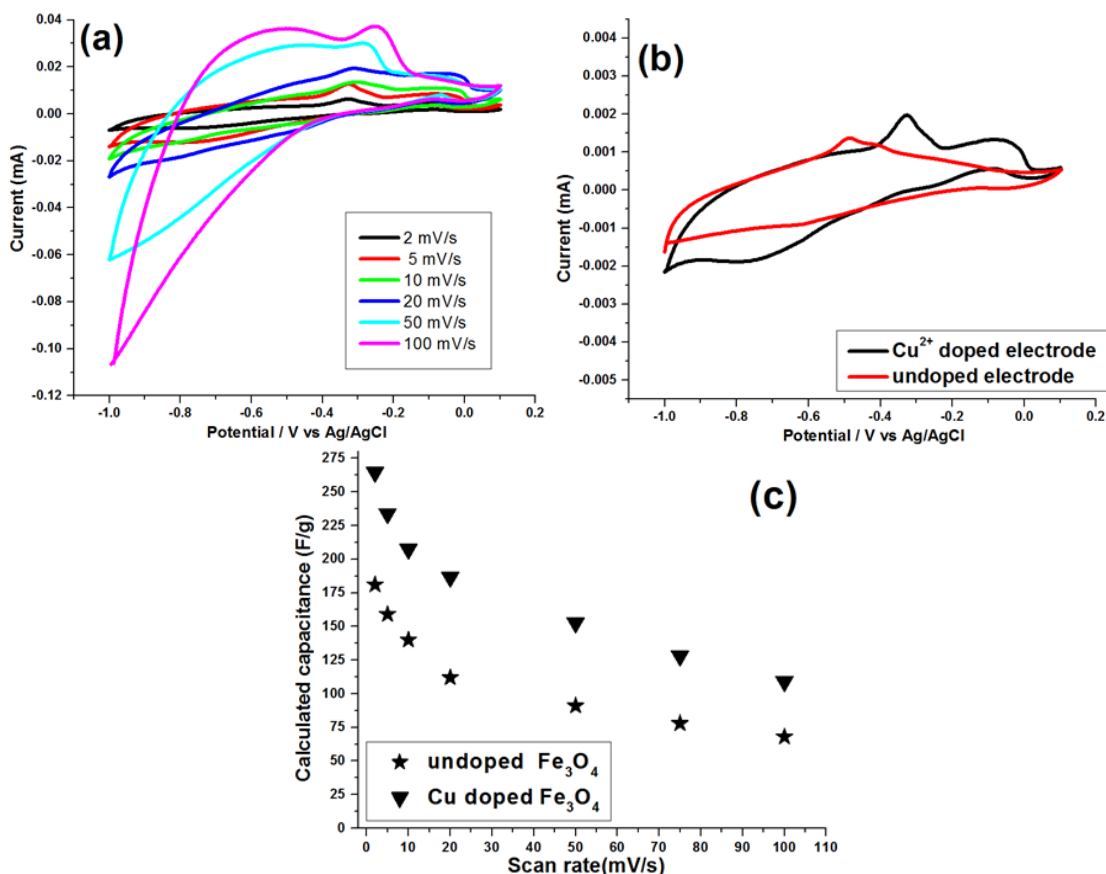
Figure 5. (a) CVs of the prepared Cu-IONPs working electrode at the various scan rates, (b) (c) CV profiles for undped and Cu^{2+} doped IONPs at the scan rate of 2 mV/s, and (c) the obtained SC values for both IONPs vs. scan rate.

For Cu-IONPs electrode, some small peaks i.e. humps are observed on CVs (Fig. 5a) as a result of redox reactions of SO_3^{2-} anions absorbed onto the surface of Cu^{2+} doped IONPs [29]:

$$2SO_3^{2-} + 3H_2O + 4e^- \leftrightarrow S_2O_3^{2-} + 6OH^- \tag{7}$$

$$S_2O_3^{2-} + 3H_2O + 8e^- \leftrightarrow 2S^- + 6OH^- \tag{8}$$

The CV tests were also provided for undoped IONPs WE, and compared with Cu^{2+} doped Fe_3O_4 NPs. Fig. 5b presents the cyclic profiles of both working electrodes at the potential sweep of 2 mV/s. It was found that the Cu^{2+} doped WE exhibits larger anodic and cathodic currents, and hence it is expected that Cu-IONPs have greater capacitances. The SC values of the both WEs were determined from their cyclic voltammetry curves using Eq. (1). Then, the SCs were plotted vs. scan rate, as shown in Fig. 5c. The obtained SC data revealed that the Cu^{2+} doped electrode are capable to give SC values as high as 264.5, 233.7, 207.4, 186.5, 152.6, 128 and 109 F g^{-1} at the scan rates of 2, 5, 10, 20, 50, 75 and 100 mV s^{-1}, respectively. Furthermore, it was obtained that the undoped WE containing Fe_3O_4 NPs are capable to provide capacitance values of 181, 159, 140, 112, 92, 83 and 68 F g^{-1} at the scan

rates of 2, 5, 10, 20, 50 and 100 mV s^{-1}, respectively. Comparing these SC values revealed that the Cu^{2+} doped Fe_3O_4 WE provide up to 45% larger SC values as compared with those of undoped WE. In fact, it is concluded that the energy storage ability of IONPs is increased by Cu^{2+} doping into the Fe_3O_4 composition. Furthermore, the obtained SC values showed the suitable capacitance of the fabricated WE from Cu^{2+} doped IONPs for use in supercapacitors.

3.2.2. Charge-discharge tests

Galvanostatic charge-discharge (GCD) curves of Cu^{2+} doped IONPs were performed at discharging loads of 0.5, 1, 2, 3 and 5 A g^{-1} and are given in Fig. 6a. These GCD profiles are very similar to those observed for IONPs electrode in Na_2SO_3electrolyte [28-31], and can be divided into two parts; first a symmetric triangular form at region of V<-0.3 V vs. Ag/AgCl, and second, nonlinear dependency of potential at region of V≥-0.3 V vs. Ag/AgCl. The first part indicates the pure EDLC behavior as a result of the charge separation at the electrode–electrolyte interface.
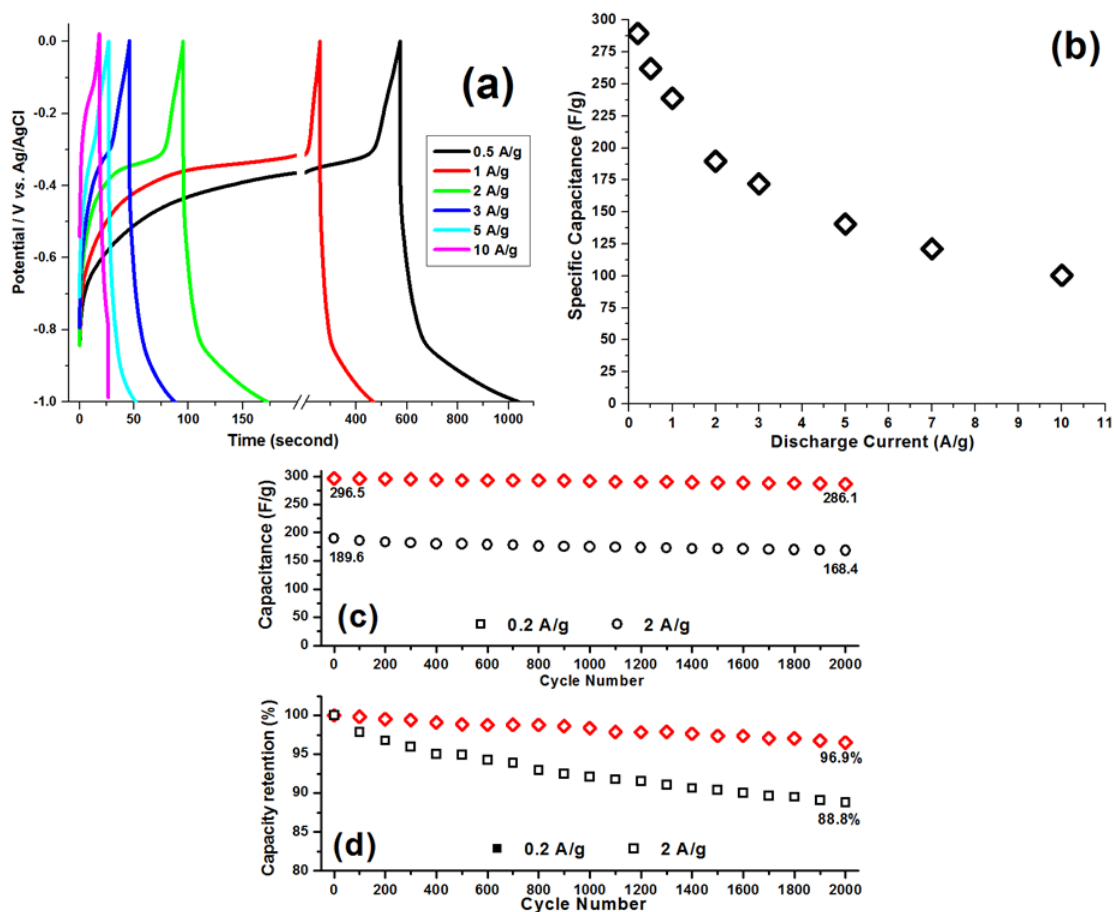
Figure 6. (a) GCD curves of Cu^{2+} doped WE and (b) its capcitances at the varoius currents of 0.2 to 5 A g^{-1}, (c) SC values and (d) SC retention for 2000 GCD test at 0.2 and 2 A g^{-1}.

The second part shows the pseudocapacitance performance of the Cu-IONPs because of the faradic reactions (Eqs.7 and 8). The SCs were calculated using Eq. (2) and the data is given in Fig. 6b.

The calculations give that the Cu^{2+} doped IONPs are capable of delivering SC values of 289.5 F g^{-1}, 262F g^{-1}, 238.8 F g^{-1}, 189 F g^{-1}, 162 F g^{-1}, 140.5 F g^{-1}, 121.1 F g^{-1} and 100.5 F g^{-1} at the discharging loads of 0.2, 0.5, 1, 2, 3, 5 and10 A g^{-1}, respectively. These findings are in agreement with SC data obtained from the CV tests (Fig. 5b), confirming the excellent super-capacitive behavior for the electro-synthesized Cu^{2+} doped Fe_3O_4 nanoparticles. Furthermore, the capacitive ability of our prepared Cu-IONPs sample is comparable with the reported SC data for the nano Fe_3O_4 electrodes in the literature; for example, 185 F/g for nanocrystals [26], 106F/g for nanowires [33], 157F/g for nanospheres [35], 268 F/g for Mn- doped spheres [36] and 120F/g for nanoparticles [42]. Comparing these SC values with our data confirmed that the SC performance of Cu-doped WE electrode is higher than those reported for pure iron oxide electrodes, and hence it is established that the charge storage of iron oxide is greatly improved by metal ion doping.

The fabricated WE was charge-discharged (2000 cycles) at the current loads of 0.2 and 2 A g^{-1} in 1M Na_2SO_3 electrolyte. The SC values and capacity retentions of the fabricated Cu-IONPs were determined during these tests. Figs. 6c and 6d represent the SCs and SC retentions vs. cycle number, respectively. It was found that the SC value of Cu^{2+} doped Fe_3O_4NPs is reduced from 296.5 F g^{-1} to 286.1 F g^{-1} after 2000 GCD cycling at a discharging current of 0.2 A g^{-1}(Fig. 6c), which exhibited about 96.9% SC retention, as seen in Fig. 6d. Also, the fabricated Cu^{2+} doped Fe_3O_4 NPs provide SC value as high as 168.4 F g^{-1} after 2000 GCD cycles at the current load of 2 A g^{-1}, which showed that the WE had SC retention of 88.8% at this discharging rate (Fig. 6d). These data confirmed the proper charge storage ability of Cu^{2+} doped Fe_3O_4 NPs. Furthermore, the energy and power densities (*E* and *P*) of the fabricated WE were determined thorough Eqs. (3 and 4) and it was observed that Cu-IONPs WE exhibits *E* and *P* values ofh as 31.7 Wh/g and 11.34kW/g, respectively. These electrochemical data provided the suitable storage performance of the fabricated Cu^{2+} doped NPs.

4. CONCLUSION

In final, a simple and facile cathodic electrodeposition method was constructed for the preparation of Cu^{2+} doped iron oxide nanoparticles (Cu-IONPs). The XRD, FE-SEM and EDS analyses proved the Fe_3O_4 crystal structure, nano-particles texture with 20 nm in size and 15%wt Cu^{2+} content of the prepared Cu-IONPs deposits. Galvanostatic charge-discharging the synthesized Cu-IONPs revealed that the Cu^{2+} doped Fe_3O_4 NPs exhibit specific capacitances values of 289.5 F g^{-1}, 262 F g^{-1}, 238.8 F g^{-1}, 189 F g^{-1}, 162 F g^{-1}, 140.5 F g^{-1}, 121.1F g^{-1} and 100.5 F g^{-1} at the discharging loads of 0.2, 0.5, 1, 2, 3, 5 and 10 A g^{-1}, respectively. It was observed that the charge storage performance of IONPs is improved (up to 30%) thought Cu^{2+} doping.

References

1. A. González, E. Goikolea, J. Andoni Barrena and R. Mysyk, *Renewable and Sustainable Energy Rev.*, 58 (2016) 1189.
2. M. Aghazadeh and M.R. Ganjali, *Ceram. Int.*, (2017) doi:10.1016/j.ceramint.2017.09.206
3. S. Kong, F. Yang, K. Cheng, T. Ouyang, K. Ye, G. Wang and D. Cao, *J. Electroanal. Chem.*, 785 (2017) 103.
4. M. Aghazadeh, R. Ahmadi, D. Gharailou, M.R. Ganjali and P. Norouzi, *J. Mater. Sci.:Mater. Electron.*, 27 (2016) 8623.
5. M. Aghazadeh, *J. Appl. Electrochem.*, 42, (2012) 89.
6. Y.X. Zhang, M. Huang, M. Kuang, C.P. Liu, J.L. Tan, M. Dong, Y. Yuan, X. Li Zhao, and Z. Wen, *Int. J. Electrochem. Sci.*, 8 (2013)136
7. M. Aghazadeh and M.R. Ganjali, *J. Mater. Sci. : Mater. Electron.*, 28 (2017) 8144.
8. A. Bello, K. Makgopa, M. Fabiane, D. Dodoo-Ahrin, K. I. Ozoemena and N. Manyala, *J. Mater. Sci.*, 48 (2013) 6707.
9. R. Poonguzhali, N. Shanmugam, R. Gobi, A. Senthilkumar, G. Viruthagiri and N. Kannadasan, *J. Power Sources*, 293 (2015) 790.
10. J. Tizfahm, M. Aghazadeh, M. G. Maragheh, M. R. Ganjali and P. Norouzi, *Mater. Lett*., 167 (2016) 153.
11. G. Xie, X. Liu, Q. Li, H. Lin, Y. Li, M. Nie and L. Qin, *J. Mater. Sci. : Mater. Electron.*, 52 (2017) 10915.
12. M. Aghazadeh, M.G. Maragheh, M.R. Ganjali, P. Norouzi and F. Faridbod, *Appl. Surf. Sci*., 364 (2016) 141.
13. M. Aghazadeh, M.R. Ganjali and P. Noruzi, *Thin Solid Films*, 634 (2017) 24.
14. C. Chen, M. Cho and Y. Lee, *J. Mater. Sci.*, 50 (2015) 6491.
15. A.A. M. Barmi, M. Aghazadeh, B. Arhami, H.M. Shiri, A. A. Fazl and E. Jangju, *Chem. Phys. Lett*., 541 (2012) 65.
16. M. Aghazadeh and M.R. Ganjali, *J. Mater. Sci.: Mater. Electron.*, 28 (2017) 11406.
17. J. Talat Mehrabad, M. Aghazadeh, M. Ghannadi Maragheh and M.R. Ganjali, *Mater. Lett*., 184 (2016) 223.
18. M. Aghazadeh, S. Dalvand and M. Hosseinifard, *Ceram. Int.*, 40 (2014) 3485.
19. J. Gou, S. Xie, Y. Liu and C. Liu, *Electrochim. Acta*, 210 (2016) 915.
20. J. Tizfahm, B. Safibonab, M. Aghazadeh, A. Majdabadi, B. Sabour and S. Dalvand, *Colloids Surf. A*, 443 (2014) 544.
21. M. Aghazadeh, M. Ghaemi, B. Sabour and S. Dalvand, *J. Solid State Electrochem*., 18 (2014) 1569.
22. M. Aghazadeh, B. Sabour, M.R. Ganjali and S. Dalvand, *Appl. Surf. Sci*., 313 (2014) 581.
23. M. Aghazadeh, I. Karimzadeh and M.R. Ganjali, *Mater. Lett*., 209 (2017) 450.
24. S.C. Pang, W.H. Khoh and S.F. Chin, *J. Mater. Sci*., 45 (2010) 5598.
25. X. Zheng, X. Yan, Y. Sun, Y. Yu, G. Zhang, Y. Shen, Q. Liang, Q. Liao and Y. Zhang, *J. Colloid Interface Sci.*, 466 (2016) 291.
26. E. Mitchell, R.K. Gupt, K. Mensah-Darkw, D.Kumar, K. Ramasamy, B.K. Gupta and P. Kahol, *New J. Chem.*, 38 (2014) 4344.
27. V. D. Nithya and N. Sabari Arul, *J. Mater. Chem.* A, 4 (2016) 10767.
28. L. Wang, H. Ji, S. Wang, L. Kong, X. Jiang and G. Yang, *Nanoscale*, 5 (2013) 3793.
29. V.D. Nithya and N.S. Arul, *J. Mater. Chem. A* 4 (2016) 10767.
30. Y. Yang, J. Li, D. Chen and J. Zhao, *ACS Appl. Mater. Interfaces*, 8 (2016) 26730.
31. Y. Z. Wu, M. Chen, X. H. Yan, J. Ren, Y. Dai, J. J. Wang, J. M. Pan, Y. P. Wang and X. N. Cheng, *Mater. Lett*., 198 (2017) 114.
32. H. Fan, R. Niu, J. Duan, W. Liu and W. Shen, *ACS Appl. Mater Interfaces*, 8 (2016) 19475.

33. X. Zhao, C. Johnston, A. Crossley and P. S. Grant*, J. Mater. Chem*., 20 (2010) 7637.
34. J. Mu, B. Chen, Z. Guo, M. Zhang, Z. Zhang, P. Zhang, C. Shao and Y. Liu, *Nanoscale*, 3 (2011) 5034.
35. K. Bhattacharya and P. Deb, *Dalton Transactions,* 44 (2015) 9221.
36. X. Yang, J. Kan, F. Zhang, M. Zhu and Z. Li, J. *Inorg. Organometal. Polym. Mater*., 27 (2017) 542.
37. X. Tang, R. Jia, T. Zhai and H. Xia, ACS App. *Mater. Interfaces*, 7 (2015) 27518.
38. T. Xia, X. Xu, J. Wang, C. Xu, F. Meng, Z. Shi, J. Lian and J.M. Bassat, *Electrochim. Acta*, 160 (2015) 114.
39. J. Ma, J. Chang, H. Ma, D. Zhang, Q. Ma and S. Wang, *J. Colloid Interface Sci*., 498 (2016) 282.
40. Q. Maqbool, C. Singh, A. Paul and A. Srivastava*, J. Mater. Chem*. C, 3 (2015) 1610.
41. S. Liu, S. Guo, S. Sun and X.Z. You, *Nanoscale*, 7 (2015) 4890.
42. P.M. Hallam, M. Gómez-Mingot, D.K. Kampouris and C.E. Banks, *RSC Adv*., 2 (2012) 6672.
43. S.Y. Wang, K.C. Ho, S.L. Kuo and N.L. Wu, *J. Electrochem. Soc*., 153 (2006) A75.
44. Q. Qu, S. Yang and X. Feng, *Adv. Mater*., 23 (2011) 5574.
45. M. Aghazadeh and M. Hosseinifard, *Ceram. Int*., 39 (2012) 4427.
46. M. Aghazadeh, I. Karimzadeh and M. R. Ganjali, *J. Mater. Sci.: Mater. Electron.*, (2017). https://doi.org/10.1007/s10854-017-7860-z.
47. M. Aghazadeh, M.G. Maragheh, M.R. Ganjali and P. Norouzi, *Inorg. Nano-Metal Chem*., 27 (2017) 1085.
48. I. Karimzadeh, M. Aghazadeh, M.R. Ganjali, P. Norouzi and T. Doroudi, *Mater. Lett*., 189 (2017) 290.
49. I. Karimzadeh, H. Rezagholipour Dizaji and M. Aghazadeh, *Mater. Res. Express*, 3 (2016) 095022.
50. I. Karimzadeh, M. Aghazadeh, M.R. Ganjali, P. Norouzi and S. Shirvani-Arani, *Mater. Lett*., 179 (2016) 5.
51. I. Karimzadeh, M. Aghazadeh, M.R. Ganjali and T. Dourudi, *Curr. Nanosci*., 13 (2017) 167.
52. M. Aghazadeh, I. Karimzadeh, M.R. Ganjali and A. Behzad*, J. Mater. Sci. : Mater. Electron.*, (2017) doi:10.1007/s10854-017-7757-x.
53. M. Aghazadeh and M.R. Ganjali, *J. Mater. Sci*., 53 (2018) 295.
54. M. Aghazadeh, I. Karimzadeh and M.R. Ganjali, *J. Mater. Sci. : Mater. Electron.*, 28 (2017) 13532.
55. M. Aghazadeh, I. Karimzadeh, T. Doroudi, M.R. Ganjali, P.H. Kolivand and D. Gharailou, *Appl. Phys. A*, 123 (2017) 529.
56. M. Aghazadeh, I. Karimzadeh and M.R. Ganjali, *Phys. Status Solidi* A, (2017) doi:10.1002/pssa.201700365.
57. C.R. De Silva, S. Smith, I. Shim, J. Pyun, T. Gutu, J. Jiao and Z. Zheng, *J. Am. Chem. Soc*., 131 (2009) 6336.
58. J. C. Parka, S. Yeo, M. Kim, G. T. Lee and J. H. Seo, *Mater. Lett*., 181 (2016) 272.
59. F. J. Douglas, D. A. MacLaren, N. Maclean, I. Andreu, F. J. Kettles, F. Tun, C. C. Berry, M. Castro and M. Murrie, *RSC Adv*., 6 (2016) 74500.
60. T. M. Thi, N. T. Huyen Trang and N. T. Van Anh, *Appl. Surf. Sci*., 340 (2015) 166.